Effect of the channel geometries on flow regimes of a viscoelastic surfactant solution in a cavity

Sato, Hideki
Kawata, Masaki
Hidema, Ruri
Suzuki, Hiroshi

(Citation)
Journal of Non-Newtonian Fluid Mechanics,310:104946

(Issue Date)
2022-12

(Resource Type)
journal article

(Version)
Accepted Manuscript

Effect of the channel geometries on flow regimes of a viscoelastic surfactant solution in a cavity

Hideki Sato[1], Masaki Kawata[1], Ruri Hidema[1]*, and Hiroshi Suzuki[1],

[1] *Department of Chemical Science and Engineering, Kobe University, Kobe 657-8501, Japan*

*Corresponding Author
Phone: +81-78-803-6657
Fax: +81-78-803-6657
hidema@port.kobe-u.ac.jp

Viscoelastic surfactant solutions exhibit a characteristic flow behavior in the cavity of a flow channel. These flows are categorized as the flow regimes of the Barus effect, bulge structure, and separation flow. The former two flow regimes sweep into the cavity, which helps increase the heat transfer efficiency of a heat exchanger with a cavity to increase the heat transfer surface. Therefore, this study visualized and quantified these characteristic flow behaviors in channels with different geometries, based on inertia and elasticity, using Reynolds number, *Re*, and Weissenberg number, *Wi*. The flow regimes were affected by both inertia and elasticity; thus, viscoelastic Mach number, *Ma*, was also useful for characterizing the flow transition. The reattachment and separation lengths of the streamlines that sweep the bottom wall of the cavity were quantified using *Re* and *Ma*. These characteristic flow lengths were characterized and modeled by dimensionless numbers in the flow regime of the Barus effect but were not uniformly characterized in the flow regime of the bulge structure. The bulge structure was an entirely unique flow regime, but it significantly reduced the recirculating regions in the cavity, which is promising for increasing heat transfer efficiency.

Keywords: Cavity flow, Deborah number, Inertia elastic instability, Viscoelastic fluid, Viscoelastic Mach number

1. Introduction

The flow behavior of viscoelastic fluids in abrupt contraction flows has been studied extensively at both macro- and micro-length scales [1-20]. Historically, the investigation of such flows was initiated to control the extrusion die of polymer melts in industrial processes and expanded to other processes that handle viscoelastic fluids [21]. The influence of fluid properties, such as extensional viscosity, elasticity, and shear-thinning, on entry flows in planar or axisymmetric abrupt contraction channels at the macro scale has been studied in a vast number of studies. The development of corner vortices, time-dependent behavior of the vortices, and pressure drop due to the vortices are affected by the fluid properties and contraction ratio of the channel [9,22-25]. In recent decades, the flow behavior of viscoelastic fluids at the microscale has garnered significant attention with the development of new technologies, such as inkjet printing, fiber spinning, micromixing, lab-on-a-chip techniques, and microrheometry [4-19,21,26-33]. The characterization of flows on a microscale has received attention not only in terms of application but also in fundamental understanding. In particular, at microscale, viscoelastic fluids reach a high Weissenberg number, Wi [-], and a low Reynolds number, Re [-], which causes purely elastic instability because of the high elasticity number, El [-] = Wi/Re [4,34-39]. Therefore, the contraction flow regimes of viscoelastic polymer solutions in microcontraction or contraction–expansion channels are often categorized in the $Wi - Re$ space. The flow developed along the slope of El in the $Wi - Re$ space by increasing the flow rates [13]. The effects of El, contraction ratio, fluid rheological properties, polymer type, polymer molecular weight, and polymer entanglement on contraction flow regimes such as lip/corner vortex growth, bending streamlines, and asymmetric flow have been intensively investigated in previous studies [13-16,18,40].

In contrast to contraction flows in the upper streams of contraction channels, studies on the expansion flows of viscoelastic fluids are relatively scarce. Expansion flows were initially studied for heat transfer enhancement and separation flow investigations. Therefore, the flow characteristics and heat transfer of Newtonian fluids or gases have primarily been studied in expansion flows [41-42]. Castro and Pinho [43] highlighted the importance of sudden expansion flow as a testbed for wall-free turbulence. They observed the recirculation bubble length in an axisymmetric sudden expansion flow and measured the mean and root mean

square of the velocity and wall pressure in the flow of water and Tylose solution. By comparing the results for water and Tylose solutions with the results of polyacrylamide solutions reported by Pak et al., they concluded that the decrease in the bubble length, caused by the drag-reducing ability of the polymers, is associated with a strong dampening of turbulence [44]. Related studies have analyzed turbulent statistics in a sudden axisymmetric expansion flow with several shear-thinning fluids, which are affected by turbulent conditions in the inlet pipe. The higher *Re* turbulence of the shear thinning fluids in the inlet pipe decreases the fluctuating velocities in the vertical and normal directions and increases the fluctuating velocities in the streamwise direction [45]. Conversely, turbulence with a lower *Re* in the inlet pipe decreases the fluctuating velocities in all directions [46]. Furthermore, contrary to expectations, a laponite solution exhibiting the characteristic properties of shear thinning, thixotropy, and yield stress does not significantly affect the mean and turbulent flows [47].

Poole and Escudier [48,49] and Poole et al. [50] conducted experimental and numerical studies on the turbulent flow of viscoelastic fluids in backward-facing steps. The increase in the reattachment length and the suppression of the strength of the recirculation regions after this step were explained by the elastic stress stored in the viscoelastic fluids. Next, the elastic stresses stored in the fluid were free to relax, resulting in the expansion of the high-velocity core, thus compressing the recirculation region in the transverse direction and elongating it in the streamwise direction. The viscoelastic effect at the inlet reduced the maximum turbulent intensity at separation, which increased turbulence anisotropy and resulted in an increased reattachment length.

In the case of micrometer-scale investigations, some studies have recently elucidated viscoelastic fluid behavior in expansion flows. Wu et al. [51] experimentally observed the flow behavior of several polymer solutions in an abrupt contraction–expansion microfluidic device and found that fluid elasticity suppresses fluid inertia-induced vortices in the expansion flow. The inertia expansion-flow vortices decrease in size when streamline bending starts in the contraction flow. These observations implied the dependence of the expansion and contraction flows on the propagation, owing to polymer extension, orientation, and relaxation in the flow. Such propagation is also important for assessing the mixing process in microfluidic devices and the viscoelastic fluid behavior in porous media.

Thus, viscoelastic fluid behavior in step contraction or expansion microfluidic devices has been studied experimentally and numerically [40,52-54]. These results imply that the extension–relaxation process of polymers or wormlike micelles in fluids may cause propagation, which induces characteristic flow behavior.

In terms of heat transfer applications, we studied the fluid behavior of viscoelastic wormlike micellar solutions in a sequence of rib and cavity flow channels, which is similar to a sequence of backward-facing step channels [55-58]. A surface with a rib and cavity helps increase the heat transfer surface in the heat exchanger. However, Newtonian fluids are likely to be stored in the cavity region as a circulating flow that is separate from the main flow, thereby prohibiting efficient heat transfer. In such a situation, viscoelastic wormlike micellar solutions are useful because viscoelastic fluids are swept into the cavity owing to the Barus effect. In our subsequent studies, we found that the expanding flow in the expansion region due to the Barus effect turns into a characteristic flow behavior: the streamline of the fluids entering the cavity, that is, the expansion region, bends toward the upstream direction. Subsequently, the fluids sweep the corner, flow downstream, and re-enter the downstream contraction region. This flow regime is known as the bulge structure [55-58]. The flow regimes in the cavity were categorized as the Barus effect, bulge structure, and Newtonian-like separation flow, which depended on the *Re*, Deborah (*De*), and *Wi* numbers. In previous studies, the separation length in the cavity was measured at each flow rate and quantified as a function of the expansion ratio and *Wi* [58]. The streamlines sweeping into the cavity fluctuated significantly over time, and the fluctuation was analyzed using particle imaging velocimetry (PIV) [55]. Three-dimensional (3D) velocity fields were also measured using PIV, which revealed the flow patterns that induced the bulge structure [55]. However, observations of flow regimes are still limited. The bulge structure has a 3D structure; that is, the expansion flow occurs in the spanwise direction, and the forward and backward flows occur in the streamwise and normal directions, respectively. Thus, the structure is affected not only by the rheological properties of the fluids but also by the channel geometry. Therefore, this study aims to clarify the effects of channel geometry on flow regimes based on dimensionless numbers related to inertia and elasticity. The channel geometry was varied by changing the cavity length, rib length, rib height, and spanwise width. The flow regimes were summarized based on dimensionless

numbers obtained from fluid properties and channel geometry. The characteristic length of each flow was normalized using a channel scale to detect the factor influencing the flow.

2. Experimental Procedures

2.1. Materials and rheological properties of the sample solution

As a cationic surfactant, Oleylbishydroxyethylmethyl ammonium chloride (trade name: Lipothoquad O/12, Lion Specialty Chemicals Co., Ltd.) was dissolved in pure water at a concentration of 2000 ppm by mixing for one day at room temperature. Subsequently, sodium salicylate was added to the surfactant solution as a counterion supplier to form wormlike micelles. The molar ratio of sodium salicylate, ξ [–], to the surfactants was adjusted at 1.5. The viscoelasticity of the wormlike micellar solution is influenced by ξ, which does not vary linearly [64]. The solution with ξ = 1.5 exhibits the highest viscoelasticity at all surfactant concentrations. The bulge structure appeared when ξ lied in the range of 0.8 to 2 and was especially pronounced when ξ = 1.5 [57]. The surfactant solution was stirred for 24 h by adding sodium salicylate and allowed to settle for one day to obtain a uniform wormlike micellar solution.

The shear viscosity, η [Pa·s], and first normal stress difference, N_1 [Pa], of the sample solution shown in Fig. 1 were measured using a shear-control rheometer with a cone-plate device of 50 mm [60]. The viscosity of the sample solution exhibited shear-thinning behavior, and the value of N_1 increased with an increasing shear rate, which is a typical behavior of wormlike micellar solutions. Furthermore, the sample solution exhibited several relaxation times. The time-dependent relaxation process of the shear stress after the sudden release of constant shear applied to the solution was measured to calculate the relaxation times of the solution using a triple exponential Maxwell model, as shown in Eq.(1) [60]:

$$\sigma = \sigma_1 e^{-t/\tau_{r1}} + \sigma_2 e^{-t/\tau_{r2}} + \sigma_3 e^{-t/\tau_{r3}}, \quad (1)$$

where σ [Pa] denotes the shear stress; t [s] is the time; τ_{r1} [s], τ_{r2} [s], and τ_{r3} [s], with $\tau_{r1} < \tau_{r2} < \tau_{r3}$, are the relaxation times related to the relaxation process

of wormlike micelles; τ_{r1} is related to the relaxation process of high-order wormlike micellar structures; τ_{r2} is related to the release of the entangled structure of the wormlike micelles; τ_{r3} represents the formation changes of micelles from wormlike to spherical micelles [60]; and σ_1 [Pa], σ_2 [Pa], and σ_3 [Pa] are the coefficients indicating the contributions of the respective surfactant structures to the initial stress. Representative values of the relaxation times are presented in Table 1.

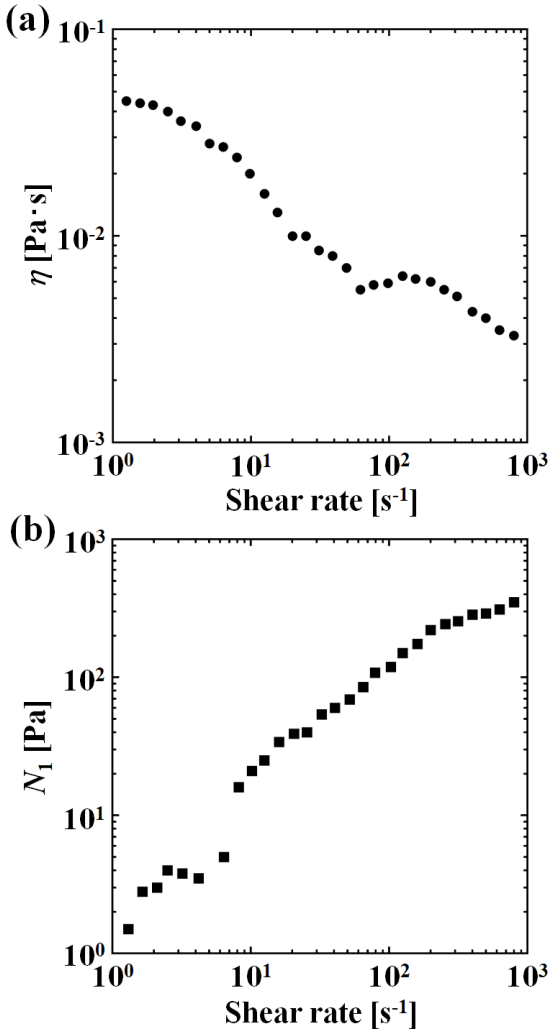

Fig. 1. Rheological properties of 2000 ppm surfactant solution with ξ = 1.5. (a) Shear viscosity and (b) first normal stress difference of the sample solution.

Table 1. Representative relaxation times of the sample solution [60].

τ_{r1} [s]	τ_{r2} [s]	τ_{r3} [s]
9.96×10^{-2}	7.77×10^{-1}	9.94

2.2. Channel geometry and flow visualization

Figure 2 shows the experimental apparatus used for the flow visualization experiments. The basic design of the experimental apparatus was proposed in a previous study [57]. A pump flowed the viscoelastic fluids from a reservoir tank into a test duct with a depth (D [m]) of 40 mm and a spanwise width (W [m]) of 75 mm, made of transparent acrylic resin. The flow rates were controlled by the pump speed in the range of 1.3–18.1 L/min. The test duct had five ribs of height H [m] and length L_r [m]. The ribs were positioned at a distance equal to the length of the cavity (L_c [m]). In the present study, the cavity length (L_c [m]), rib length (L_r [m]), rib height (H [m]), and spanwise width (W [m]) were varied, as summarized in Table 2. The four main groups of channels were named as Channels A, B, C, and D. These groups also had varying channel heights H. The effects of these channel geometries on the flow regimes were visualized. Flow visualization was performed in the fourth cavity of the channel, where the flow stabilized after a sufficient entry length. The characteristic flow behaviors were visualized with red ink injected from the top of the channel or with tracer particles (diameter 0.1 mm) made of ion-exchange resin (DIAION HP20, MITSUBISHI CHEMICAL) and were recorded by a video camera (HC-W850M, Panasonic) with a resolution of 1280 × 720 pixels at a shutter speed of 1/500 s and time interval of 1/60 s.

To characterize the flow regimes, the zero-shear Re [–] and Wi [–] are defined as follows: Re is the ratio of the inertial to viscous forces [36,37]. Wi represents the ratio of elastic to viscous forces, i.e., the dimensionless strain rate [36, 65].

$$Re = \frac{\rho U_m (D-H)}{\eta_0} \tag{2}$$

$$Wi = \tau_{r2} \frac{U_m}{(D-H)}, \tag{3}$$

where ρ [kg/m^3], U_m [m/s], τ_{r2} [s], and η_0 [Pa· s] represent the fluid density, flow velocity in the narrow flow path, second relaxation time, and zero-shear viscosity, respectively. η_0 was obtained at a shear rate of 10^0 1/s by extrapolating the three plots in the lowest shear rate range. Previous studies have shown that the second

relaxation time strongly affects the behavior of fluid separation from the bottom of the cavity; thus, τ_{r2} was used to calculate *Wi* [60].

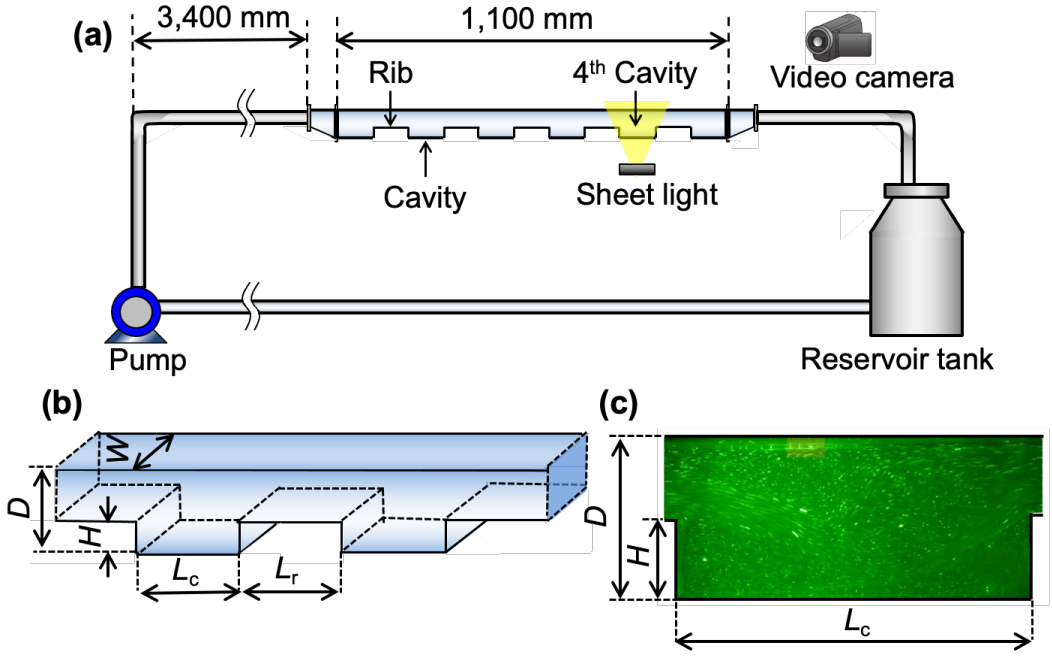

Fig. 2. Schematic of (a) The experimental apparatus. (b) Close up of the test section for flow visualization. (c) Example of a flow in the cavity recorded by a video camera.

Table 2. Detailed dimensions of each channel named A to D.

Channel	*W* [mm]	*D* [mm]	L_c [mm]	L_r [mm]	*H* [mm]
A	75	40	100	100	15 20 25 30
B	75	40	125	100	15 20 25 30
C	75	40	100	75	15 20 25 30
D	50	40	100	100	15 20 25 30

3. Results and Discussion

3.1. Flow regimes observed in the cavity

Figure 3 shows examples of the flows visualized in the fourth cavity of each flow channel at several flow rates. Three types of flow regimes mentioned in the introduction section are shown; the expanding flow in the cavity arising from the Barus effect, the characteristic bending and sweeping flow named as the bulge structure, and the separation flow that does not sweep into the cavity causing the circulating stagnation area in the cavity. A relatively low *Re* induces the flow arising from the Barus effect. Subsequently, the bulge structure and the separation flow appear by increasing *Re*. However, not only *Re* but also channel geometry and fluids properties affect the flow regime.

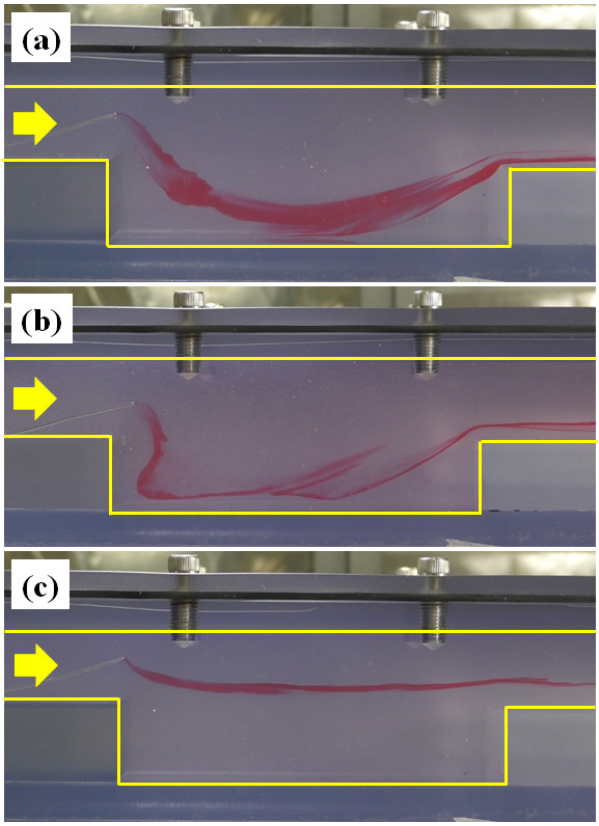

Fig. 3. Characteristic flow regimes of (a) Barus effect observed at $Re = 18.2$ and $Wi = 1.77$, (b) bulge structure observed at $Re = 31.1$ and $Wi = 3.04$, and (c) separation flow observed at $Re = 53.5$ and $Wi = 5.20$ in the cavity of Channel A with $H = 20$ mm. The flow was visualized by red ink injected into it.

3.2. Flow regimes on Re–Wi space

To characterize the effects of the elasticity and inertia of fluids on the flow in each channel [62,63], the flow regimes were summarized in the *Wi* – *Re* space, as shown in Fig. 4. Each experimental point in each channel corresponds to the elasticity number, *El* [-] = *Wi*/*Re*, which is the ratio of elasticity and inertia [20, 36, 37]. By definition, *El* is not affected by the channel geometry of channels A through D, but by the channel height. The dotted line in Fig. 4 indicates each *El* in the experimental condition. Flow conditions, such as the Barus effect, bulge structure, and separation flow, were determined by the balance of both the inertial and elastic forces. Therefore, the development of the flow was observed on the slope of *El* by increasing the flow rates. A flow affected by the Barus effect was observed in the region where both *Wi* and *Re* were small. The flow became a bulge structure in the intermediate regions of *Re* and *Wi*. In addition, a bulge structure is repeatedly created and disappears on a timescale of approximately 10 s [55]. Subsequently, a separation flow occurred in the region where both *Wi* and *Re* were relatively large. This tendency was similar for all the channels with different rib heights.

The critical *Re* at which the flow transitions from the Barus effect to the bulge structure decreases with an increase in the rib height. As *Re* is defined in Eq. (2), the same *Re* value results in a larger U_m when *H* is higher. An increase in velocity along a narrow flow path induces unstable flows. However, the unstable flow was not by velocity fluctuation in the streamwise direction. Although the velocity fluctuations were occurred in a flow, we have confirmed the fluctuation intensity in streamwise direction was less than 2%. Therefore, the viscoelastic Mach number *Ma* [–] is a suitable dimensionless parameter for evaluating the onset of unstable flow. *Ma* is the ratio of the local velocity to the speed of the viscoelastic wave and is defined as follows:

$$Ma = \sqrt{ReWi} \tag{4}$$

In general, when *Ma* > 1, we would expect some sort of transition in the flow. It has been reported that the speed of the base flow exceeds that of the elastic wave [37], resulting in highly strained dispersed components such as worm-like micelles or polyemrs, creating a secondary flow with curved streamlines in the base flow that becomes unstable. In this study, the transition from the Barus effect to a bulge

structure occurred when $Ma = 6$. The bulge structure is considered a secondary flow owing to the mixed effects of the inertia and elasticity of the fluids. In addition, the bulge structure repeatedly appeared and disappeared on a timescale of several seconds to 10 s [55].

To observe the Barus effect and the bulge structure, the relaxation time τ_{r2} of the fluids should be shorter than the residence time in the cavity. This is because the fluids require some time to penetrate the cavity before reaching the next rib, which may be due to the release of the entangled structure of the wormlike micelles. Thus, to compare the ratio of the relaxation time of the solution to the residence time in the cavity, *De* [–] is expressed as follows [36, 65]:

$$De = \tau_{r2} \frac{U_\mathrm{m}}{L_\mathrm{c}} \tag{5}$$

De is defined as a function of relaxation time τ_{r2}, fluid velocity U_m, and cavity length L_c. $U_\mathrm{m}/L_\mathrm{c}$ represents the observation time for the fluid in the cavity. The second relaxation time of the fluids was used here as well as in the calculation of *Wi*. As shown in Fig. 4, *De* describes the transition from the bulge structure to the separation flow. A bulge structure was observed in the regions of $Ma > 6$ and $De < 1$ ($Ma < 16$ for Channels A, C, and D and $Ma < 20$ for Channel B), and separation flow was observed in the region of $De > 1$ ($Ma > 16$ for Channels A, C, and D and $Ma > 20$ for Channel B). This tendency was similar in all channels, except Channel C with H=15 mm, where the bulge structure did not appear. These results indicate that a sufficient shear rate and a certain period of time are required to enhance the wormlike micelles, which induce the bulge structure. The enhancement and relaxation processes of micelles caused by channel geometries influence the flow regimes.

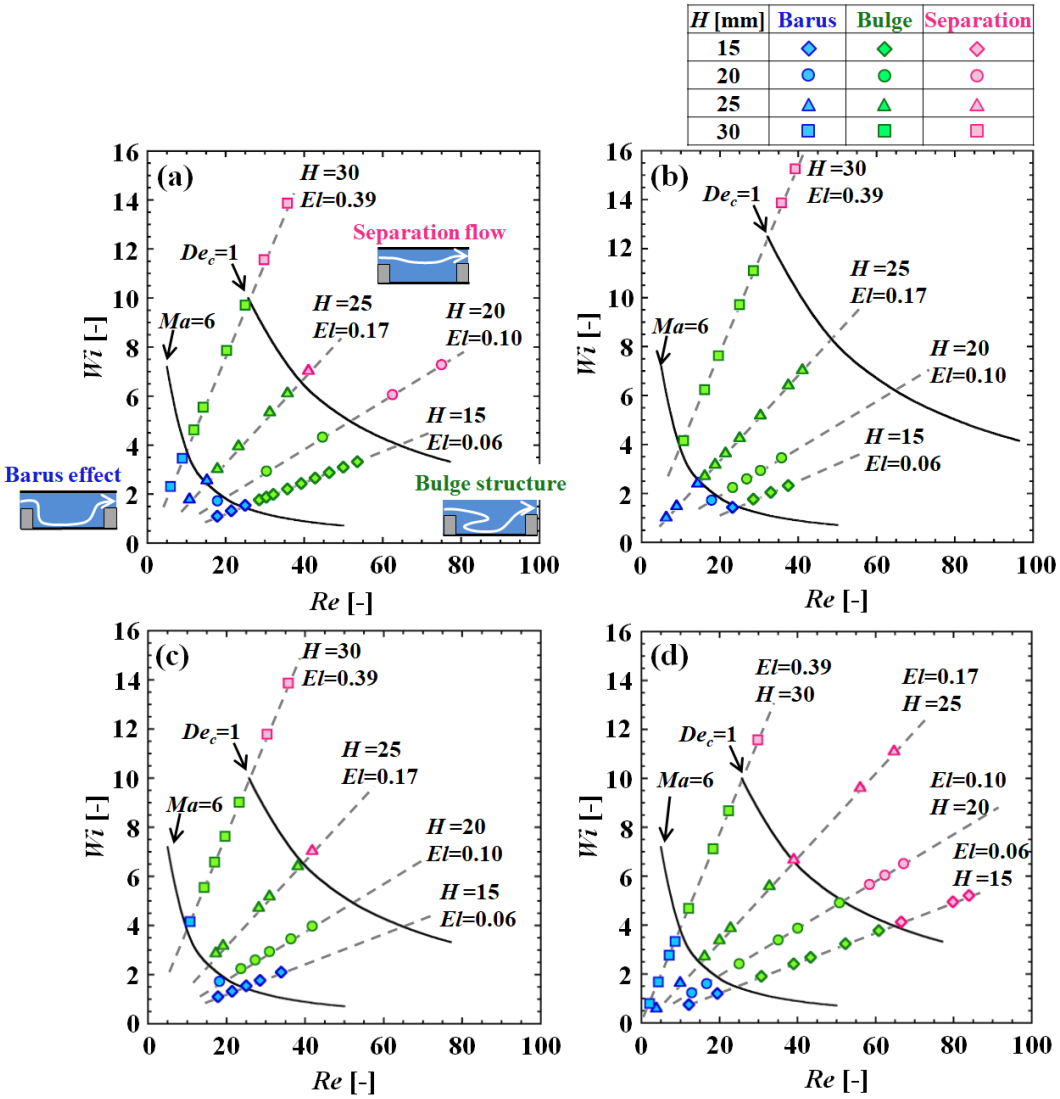

Fig. 4. Flow regime in (a) Channel A, (b) Channel B, (c) Channel C, and (d) Channel D with H = 15 – 30 mm summarized on Re – Wi space. The dotted line corresponds to each El in each channel with each H. Two solid lines show the transition conditions defined by Ma = 6 (De = 0.374) and De_C = 1 (Ma = 16).

3.4. Reattachment and separation characteristics of the viscoelastic fluid in the cavity

To precisely characterize the flow regimes, the reattachment length (X_r [m]) and separation length (X_s [m]) were defined. X_r is the distance from the bottom-left edge of the cavity to the position where the flow is attached to the bottom, as shown in Figs. 5 – 8. The flow sweeps at the bottom of the cavity and converges again to flow over the rib. X_s is the distance from the position at which the flow separates from the bottom to the right edge of the cavity, as shown in Figs. 9 – 12.

Figure 5(a) shows the variation in X_r normalized by the cavity length L_c plotted as a function of *Re* for Channel A. Here, *Re* is influenced by the rib height *H*; the increase in *H* leads to a decrease in *Re*, which is according to the definition of *Re*, as described in Eq. (2). The value of X_r/L_c is influenced by the flow regime of the Barus effect and the bulge structure. In the area where the Barus effect was observed, X_r/L_c increased with increasing *Re*, which is commonly observed in viscoelastic fluids in cavities [57]. When the flow transitioned to the bulge structure, X_r/L_c immediately decreased, a characteristic phenomenon of the bulge structure in which the upstream flow occurred in the cavity and the flow swept at the bottom of the cavity. Because the bulge structures fluctuated as they appeared and disappeared over time, the error bars showing the maximum and minimum values of the bulge structure were wide. In both the flow regimes, X_r/L_c increased slightly with increasing *Re*. After the appearance of the bulge structure, the flow finally reached separation flow.

Figure 5(b) shows X_r/L_c as a function of *Ma* for Channel A, which describes the transition points from the Barus effect to the bulge structure. The variation in X_r/L_c was characterized by *Ma*, regardless of the difference in *H*. Figures 5(c) and (d) show X_r normalized by *H* as a function of *Re* or *Ma* for Channel A. In Fig. 5(c), the effect of *Re* on the increase in X_r/H in both flow regimes is clearly observed. However, the impact of *H* on X_r was smaller than that on L_c, which was unexpected.

Figures 6 shows X_r/L_c and X_r/H as a function of *Re* and *Ma* for Channel B. L_r of Channel B has the same length as that of Channel A, and L_c of Channel B is longer than that of Channel A. The variation in X_r in the cavity of Channel B is characterized better by the function of *Ma* than that of *Re*. X_r/L_c and X_r/H are slightly increased by increasing *Ma* in the flow regime dominated by Barus effect, and X_r/L_c and X_r/H decrease in the bulge structure region. However, the depression at Ma = 1, and the subsequent increase of these values until De =1 are weaker than the tendency observed in Channel A. When the L_c is small, X_r in the cavity may be influenced by the accelerating flow occurring at the cavity outlet. Thus, X_r may be stretched to the outlet. However, this effect becomes weaker when L_c is large. This might be the reason for the smaller value of X_r in Channel B than that in Channel A.

Figure 7 shows X_r/L_c and X_r/H as a function of *Re* and *Ma* for Channel C. The variations seen in X_r/L_c and X_r/H are very small. The difference in Channel C

is that the shorter L_r than the other channels. As can be seen in Fig, 4(c), enough shear rates in a certain period of time is required to enhance wormlike micelles that causes Barus effect and the bulge structure. These effects are weak in Channel C, leading to the small variations of X_r/L_c and X_r/H.

Figure 8 shows X_r/L_c and X_r/H as a function of *Re* and *Ma* for Channel D. Channel D has the same dimensions as Channel A except for the spanwise width, *W*. The tendency of the variation is similar to that of Channel A as compared to Channel B and C, which indicates that the effects of *W* on the flow regime is smaller than the other dimensions.

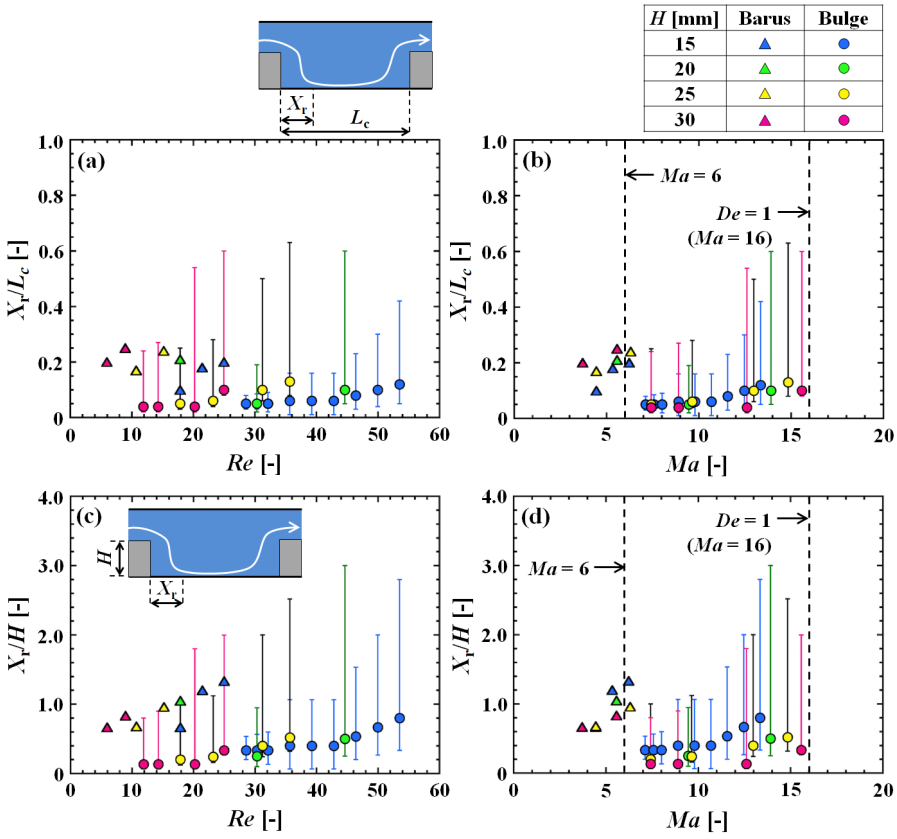

Fig. 5. Reattachment length X_r normalized by the cavity length L_c or by the cavity height *H* plotted as a function of *Re* or *Ma* in Channel A with $H = 15 – 30$ mm.

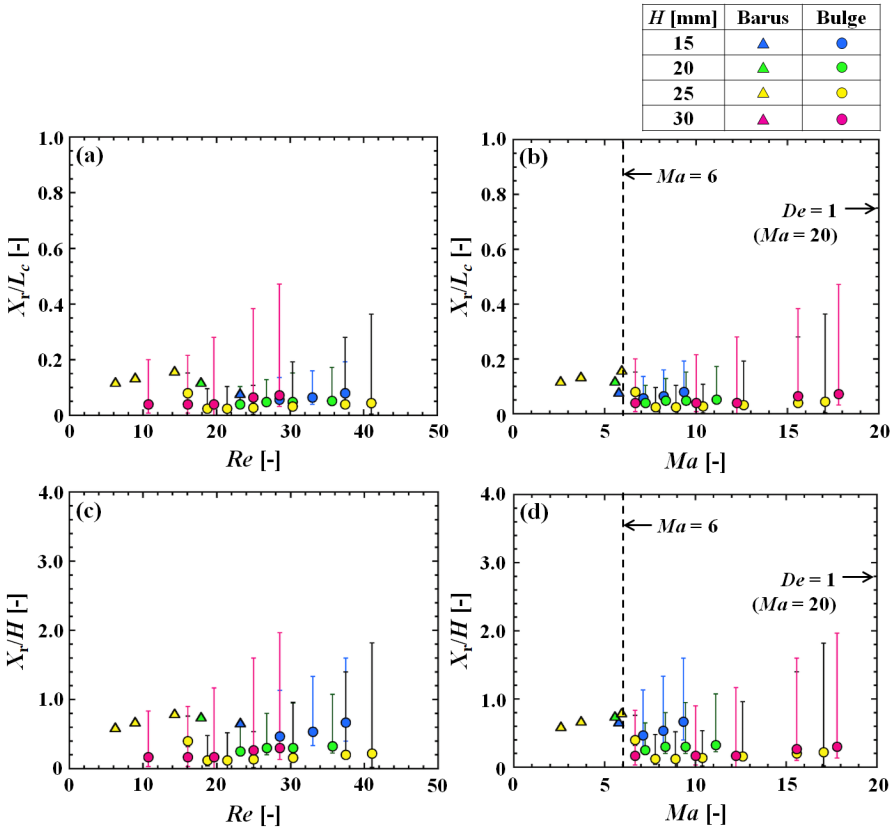

Fig. 6. Reattachment length X_r normalized by the cavity length L_c or by the cavity height H plotted as a function of Re or Ma in Channel B with H = 15 – 30 mm.

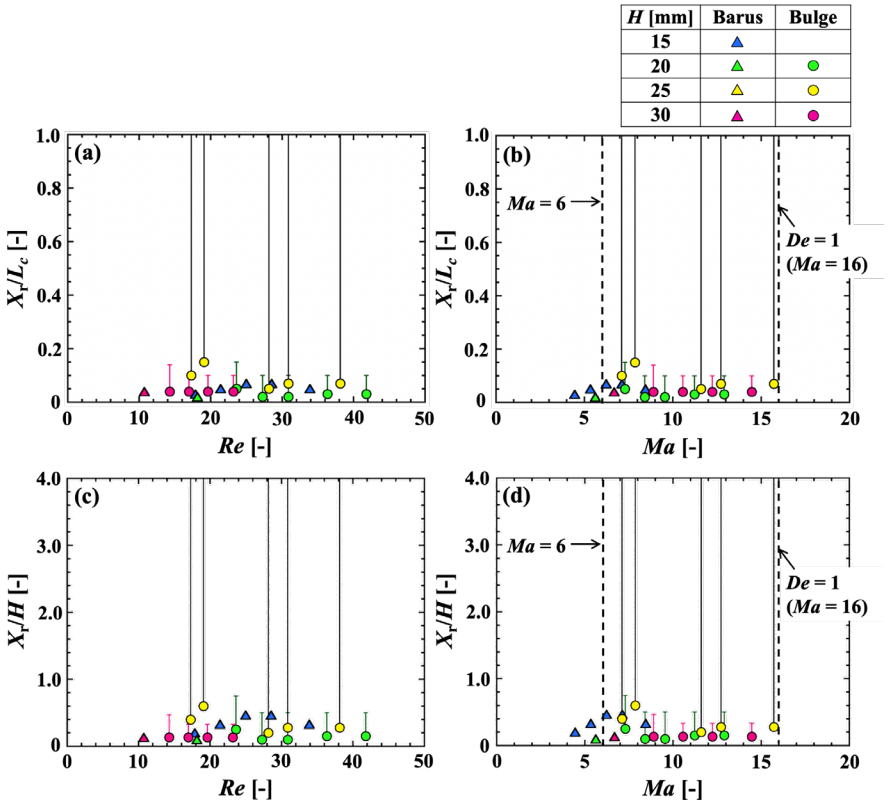

Fig. 7. Reattachment length X_r normalized by the cavity length L_c or by the cavity height H plotted as a function of Re or Ma in Channel C with H = 15 – 30 mm.

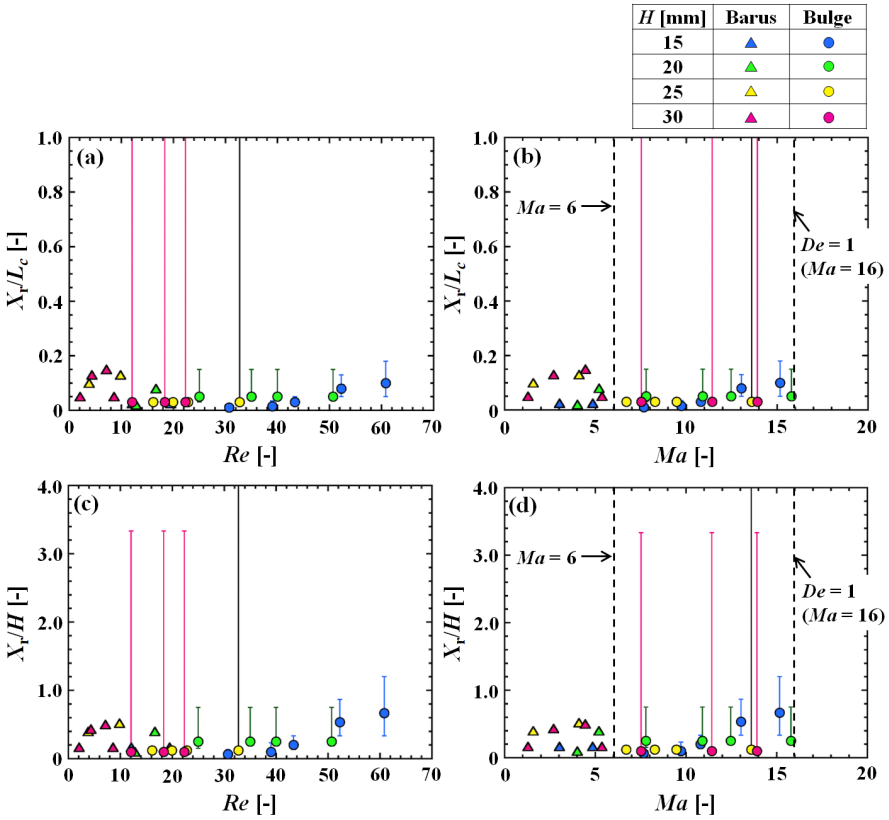

Fig. 8. Reattachment length X_r normalized by the cavity length L_c or by the cavity height H plotted as a function of Re or Ma in Channel D with H = 15 – 30 mm.

Figures 9 – 12 show the variation in X_s normalized by L_c or H as a function of Re or Ma for Channels A to D. In addition to X_s, the error bars showing the maximum and minimum values were added to the flow regime of the bulge structure. The development of X_s was better characterized as a function of Ma than that of Re in all channels. Fig. 11 shows that, compared with the other channels, the variation in X_s fluctuated significantly in the case of Channel C. This was again due to the short L_r that did not allow sufficient shear rates to be added to the flow to enhance wormlike micelles.

In addition to X_r, the flow transition from the Barus effect to the bulge structure tended to decrease X_s in all channels, as shown in Figs. 9 – 12. However, the effects of the flow regimes and Ma on X_s were smaller than those on X_r. Apparently, X_s was affected by H; thus, X_s/H showed similar values in all channels with different H values compared to X_s/L_c. As X_s was not normalized well by L_c, the effects of L_c on X_s seemed small. However, we also noticed a slight influence of L_c on X_s when we compared X_s/H in Channels A, C, and D (shown in Fig. 9(d), Fig. 11(d), and Fig. 12(d)) to X_s/H in Channel B, as shown in Fig. 10(d). In the case of

Channel B, which had a longer L_c, X_s/H collapsed well on the curve as a function of *Ma* compared with the other channels. This implies that X_s is solely affected by H when L_c is sufficiently long. However, when L_c became short, the accelerating flow at the outlet of the cavity influenced the flow, which expanded X_s upstream. We speculate that an interaction between the flow entering and leaving the cavity may occur, which influences X_r and X_s. Additionally, the effect of W on X_s was relatively small because the tendency of X_s variation in Channel A was similar to that in Channel D, as shown in Figs. 9 and 12.

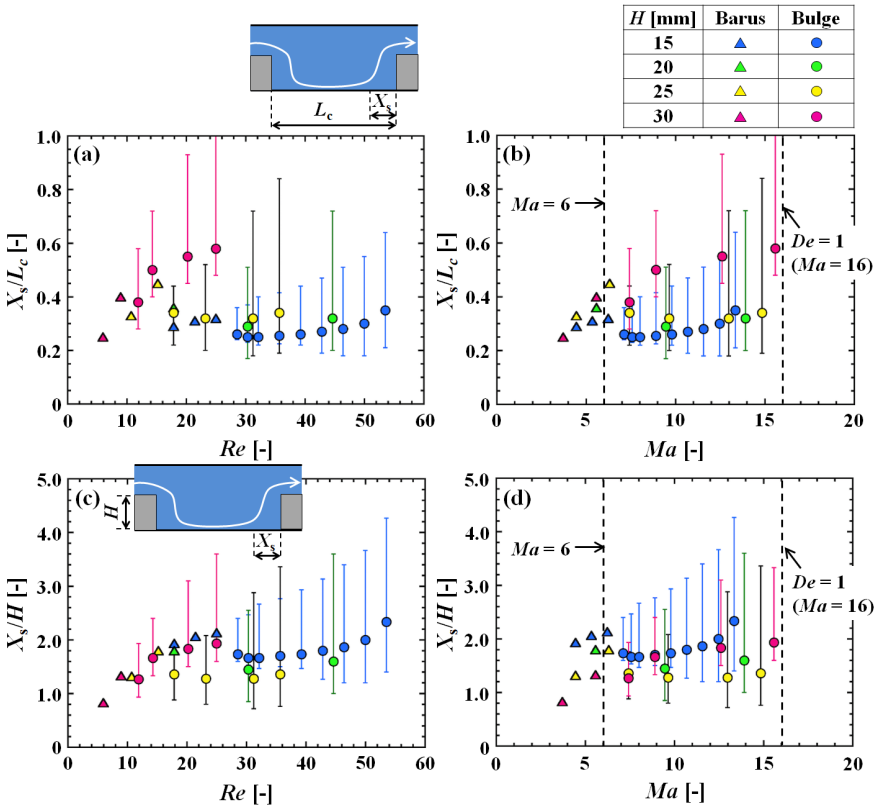

Fig. 9. Separation length X_s normalized by the cavity length L_c or by the cavity height H plotted as a function of *Re* or *Ma* in Channel A with H = 15 – 30 mm.

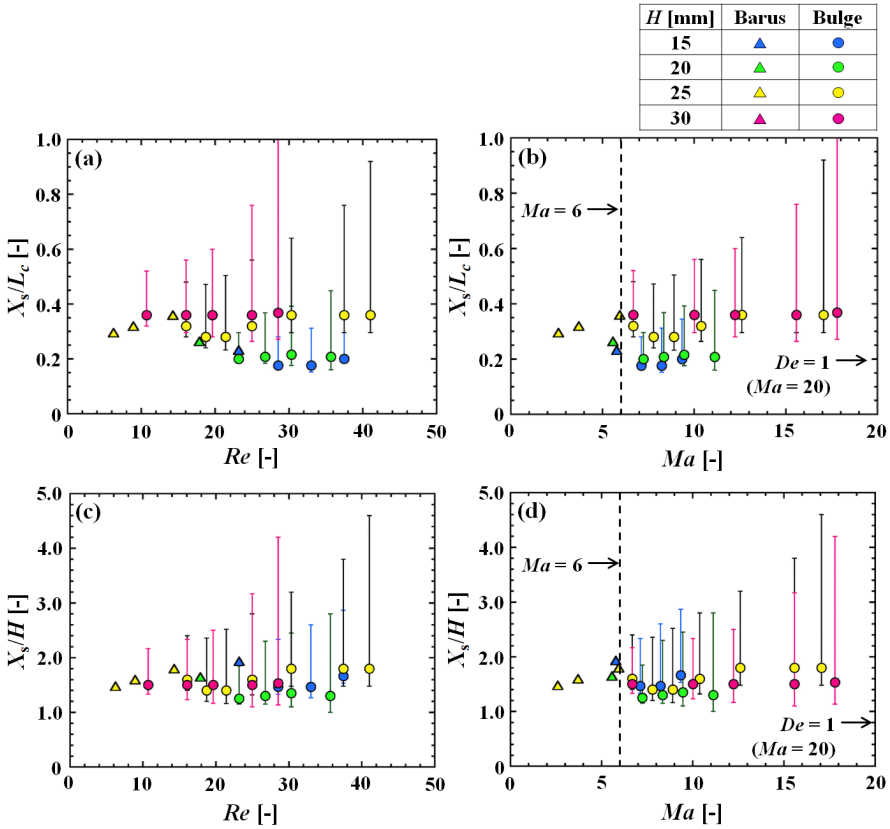

Fig. 10. Separation length X_s normalized by the cavity length L_c or by the cavity height H plotted as a function of Re or Ma in Channel B with H = 15 – 30 mm.

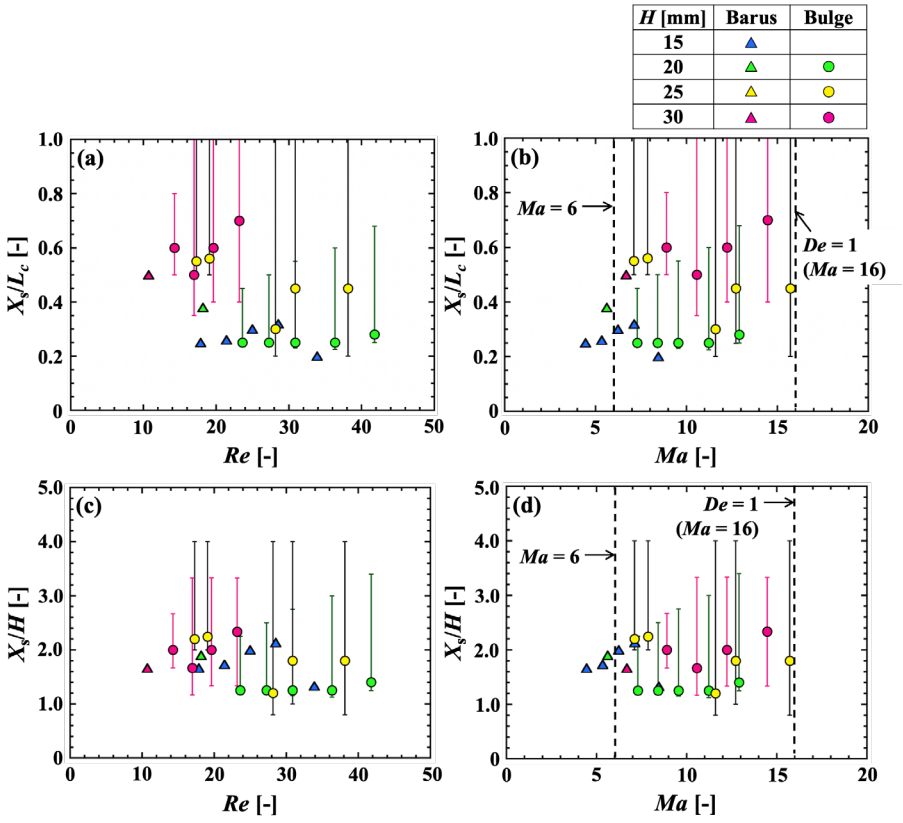

Fig. 11. Separation length X_s normalized by the cavity length L_c or by the cavity height H plotted as a function of Re or Ma in Channel C with H = 15 – 30 mm.

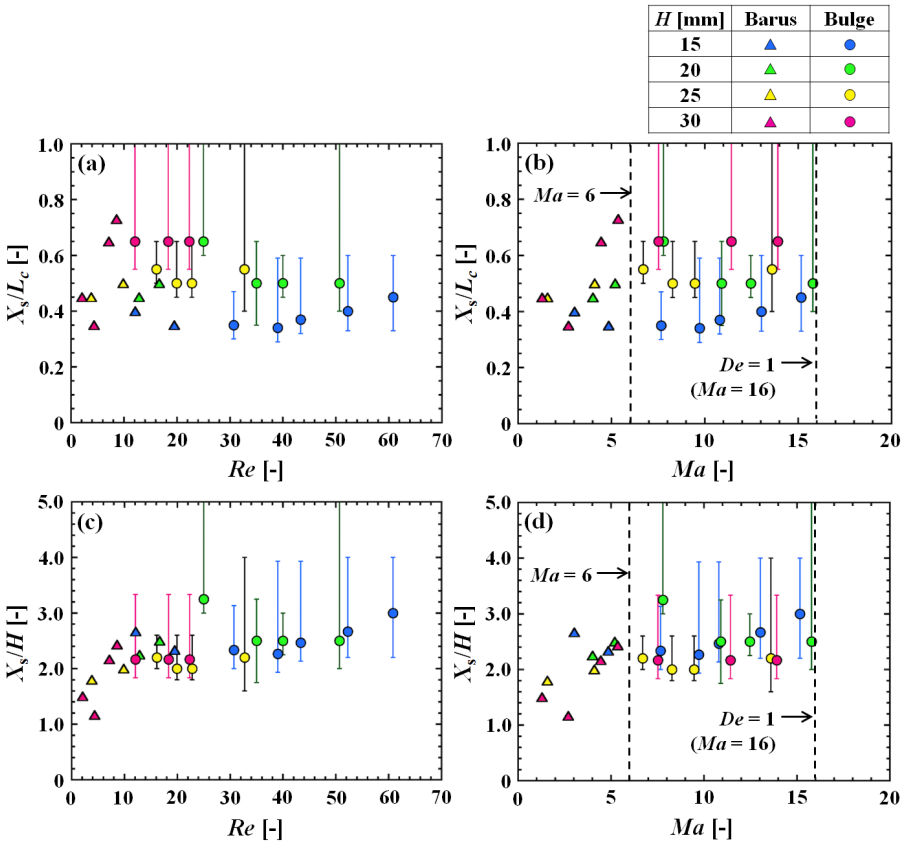

Fig. 12. Separation length X_s normalized by the cavity length L_c or by the cavity height H plotted as a function of Re or Ma in Channel D with H = 15 – 30 mm.

Here, we consider the factors that appear as effects of H to describe the development of X_s in the flow regime affected by the Barus effect. Figure 13 shows a schematic of the flow showing X_s and the mean velocities at the two positions. Here, position A is the point at which separation begins and position B is the contraction point. The velocity at position B was U_m, as described in Eqs. (2) and (3), and the mean velocity at position A was denoted as U_0. The variation in momentum in the focused area between positions A and B is described by Eq. (6). The force applied to the flow in the focused area is determined using Eq. (7) as follows:

$$\rho U_{\mathrm{m}}^2(D-H)-\rho U_0^2 D \qquad (6)$$

$$(P_A-\tau_{\mathrm{xx}}|_{\mathrm{A}})D-(P_B-\tau_{\mathrm{xx}}|_{\mathrm{B}})(D-H)-P_B H-\tau_{\mathrm{xy}}X_{\mathrm{s}}, \qquad (7)$$

where P_A [Pa·s] and P_B [Pa·s] represent the pressures at positions A and B, respectively, and $\tau_{\mathrm{xx}}|_{\mathrm{A}}$ [Pa·s] and $\tau_{\mathrm{xx}}|_{\mathrm{B}}$ [Pa·s] are the normal stresses at each

position. Eq. (6) is equivalent to that in Eq. (7). Thus, Eq. (8) can be obtained as follows.

$$(P_A - \tau_{xx}|_A)D - (P_B - \tau_{xx}|_B)(D - H) - P_B H - \tau_{xy} X_s = \rho U_m^2 (D - H) - \rho U_0^2 D \quad (8)$$

Eq. (8) is solved to consider the factor that defines X_s. First, we assume the Bernouilli equation to describe pressure variations, as expressed in Eq. (9):

$$P_A - P_B = \frac{1}{2}\rho U_m^2 - \frac{1}{2}\rho U_m^2 \left(\frac{D-H}{D}\right)^2 = \frac{1}{2}\rho U_m^2 \frac{H}{D}\frac{2D-H}{D} \quad (9)$$

Eq. (10) is derived by substituting Eq. (9) into Eq. (8). Here, because Trouton's ratio that is the ratio of extensional viscosity to shear viscosity of the fluids is 20, $\tau_{xx}|_A$ and $\tau_{xx}|_B$ are estimated as ten times larger than τ_{xy} for laminar flow [66]. Thus, the term $-\tau_{xy} X_s$ is smaller compared to the normal stresses $\tau_{xx}|_A$ and $\tau_{xx}|_B$, therefore, it is omitted.

$$\tau_{xx}|_B (D - H) - \tau_{xx}|_A D = \rho U_m^2 (D - H)\frac{H}{D} - \frac{1}{2}\rho U_m^2 \frac{H}{D}\frac{2D-H}{D} D = -\frac{1}{2}\rho U_m^2 \frac{H^2}{D} \quad (10)$$

Subsequently, the normal stress is assumed using the Maxwell model, as expressed in Eq. (11).

$$\tau_{xx} = \frac{\eta}{\lambda}\frac{1}{1-2\dot{\varepsilon}\lambda} \quad (11)$$

The term $\dot{\varepsilon}$ is obtained as the mean extensional rate in the focused area, which is assumed to be the extensional rate at positions A and B.

$$\dot{\varepsilon} = \frac{U_m}{X_s}\frac{H}{D} \quad (12)$$

Eq. (12) can be substituted into Eq. (11). Subsequently, X_s can be obtained as a function of *Wi* and *Re*.

$$\frac{\eta}{\lambda}\frac{1}{1-2\frac{U_{\mathrm{m}}H}{X_{\mathrm{s}}D}\lambda}H=\frac{1}{2}\rho U_{\mathrm{m}}^{2}\frac{H^{2}}{D} \qquad (13)$$

$$\frac{X_{\mathrm{s}}}{H}=\frac{Wi^{2}Re\frac{D-H}{D}}{\frac{1}{2}WiRe-\frac{D}{D}}, \qquad (14)$$

where

$$Wi=\lambda\frac{U_{\mathrm{m}}}{D-H}, \text{ and } Re=\frac{\rho U_{\mathrm{m}}(D-H)}{\eta} \qquad (15)$$

Figure 14 shows X_s/H observed in each channel as a function of $(Wi^2\,Re\,\frac{D-H}{D})/(\frac{1}{2}\,Wi\,Re-\frac{D}{H})$ as derived in Eq. (14). As expected, when the flow regime is dominated by the Barus effect, X_s/H follows the value derived by Eq. (14); thus, the separation flow is affected by the extensional characteristics of fluids. Here, in the case of Channel D, X_s/H slightly deviates from Eq. (14) in the flow regime dominated by the Barus effect. We consider the slight discrepancy reflects the effect of spanwise width. In the derivation of Eq. (14), the variation of spanwise width was not considered as the model was 2D. Therefore, it is possible that the small deviation occurs. Conversely, the mean value of X_s/H highly deviates from Eq. (14) in the bulge structure region, and the flow regimes are not solely explained by the extensional characteristics as described above.

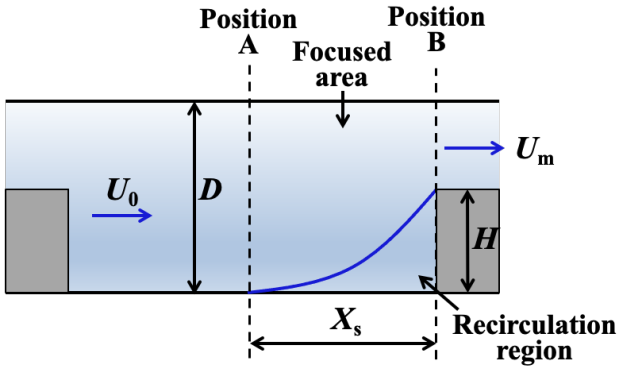

Fig. 13. Schematic of the focused area in the cavity including the separation length X_s.

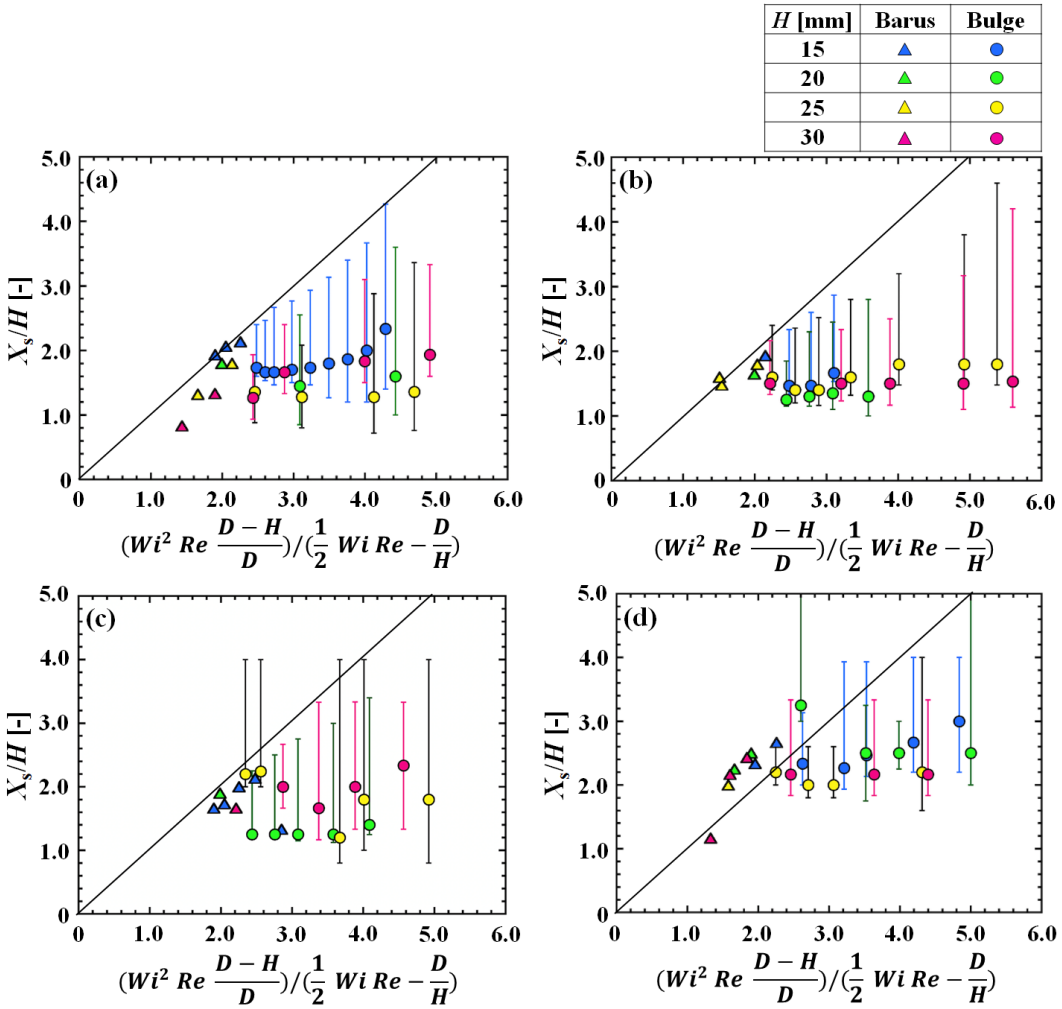

Fig. 14. Value of X_s/H in (a) Channel A, (b) Channel B, (c) Channel C, and (d) Channel D with H = 15 – 30 mm plotted as a function of $(Wi^2\ Re\ \frac{W-H}{W})/(\frac{1}{2}\ Wi\ Re - \frac{W}{H})$, shown by the solid line.

Figures 15 – 18 show the length of the bulge structure (X_b [m]) for all the channels. X_b normalized by L_c as a function of *Re* and *Ma* is shown in Figs. 15 – 18 (a) and (b), respectively. The bulge structures repeatedly appear and disappear; thus, the error bars vary from zero to the maximum value. X_b/L_c increases with increasing *Re* and *Ma*, and this phenomenon is affected by both inertia and elasticity. In addition to the effects of inertia and elasticity, an increase in H induces an increase in X_b, which indicates that sufficient cavity depth is required to produce the flow regime of the bulge structure. To verify the effects of H on X_b, X_b/H as a function of *Re* and *Ma* is shown in Figs. 15 – 18 (c) and (d). Figures 15 – 18 (c) show that X_b/H collapsed at a similar value within a certain range of *Re*, which clarifies the significant impact of H on X_b. The variation in X_b/H was also

summarized as a function of *Ma*; X_b/H exhibited a similar value in each channel, which increased with *Ma*. Again, the tendency was slightly different in Channel C, but this may be due to the shorter L_r.

The results shown in Figs. 8 – 18 demonstrate that the flow regimes in the cavity were affected by the inertio-elastic effects represented by *Ma*. The separation flow represented by X_s in the Barus effect region was dominated by the extensional characteristics of the flow appearing as an effect of *H*. The effects of *H* were clearly observed in the length of the bulge structure, which required sufficient depth in the cavity.

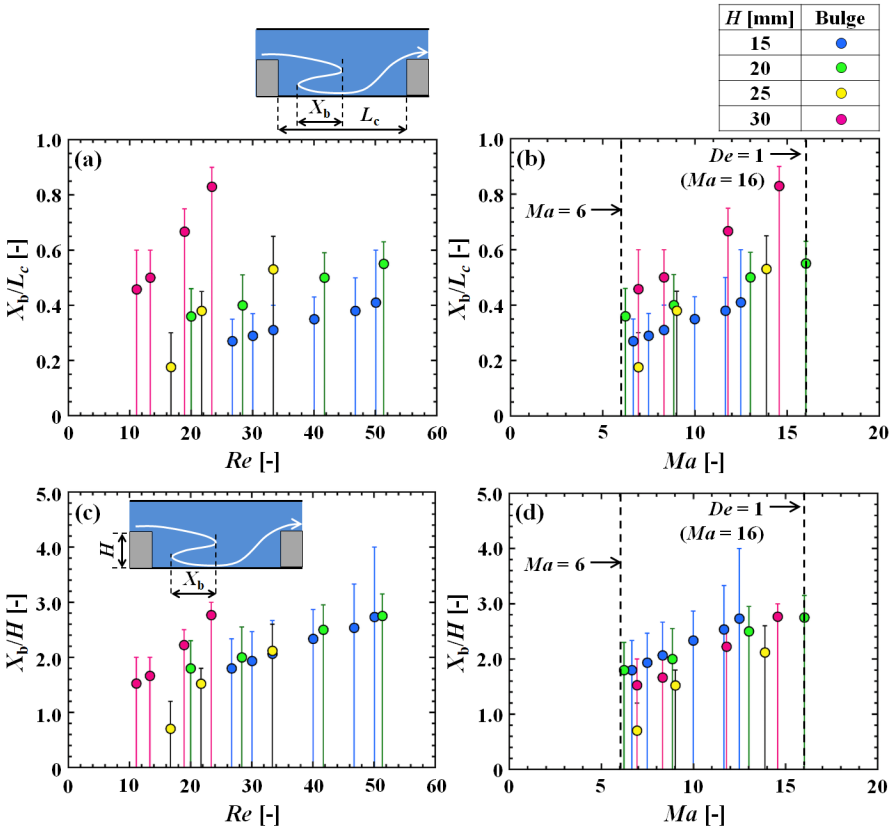

Fig. 15. Length of the bulge structure X_b in Channel A with H = 15 – 30 mm normalized by L_c and H plotted as a function of *Re* and *Ma*.

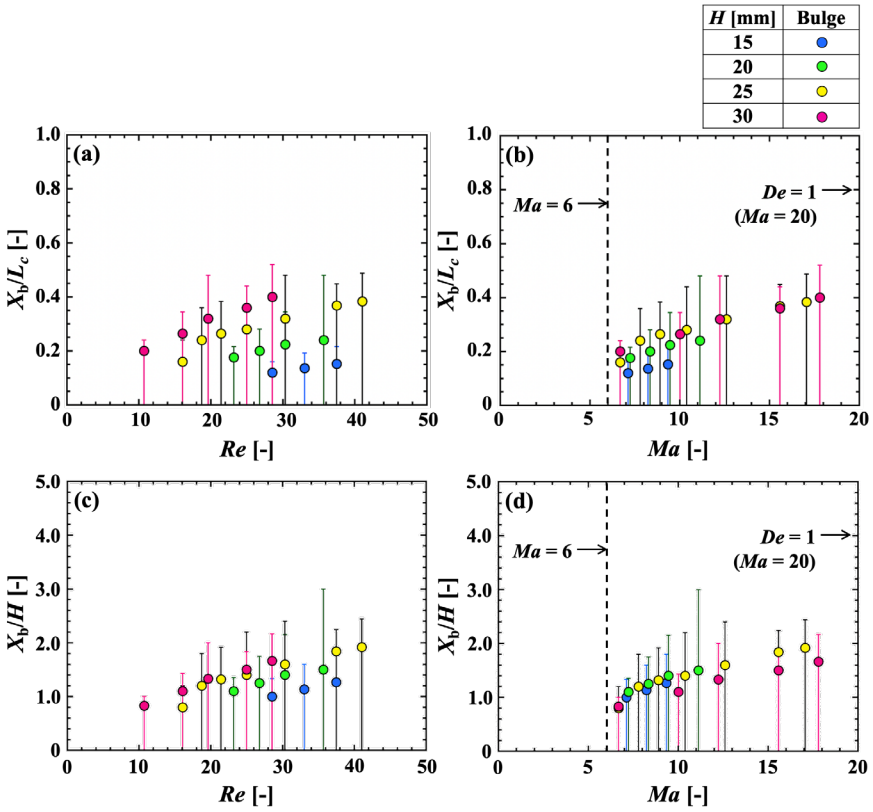

Fig. 16. Length of the bulge structure X_b in Channel B with H = 15 – 30 mm normalized by L_c and H plotted as a function of Re and Ma.

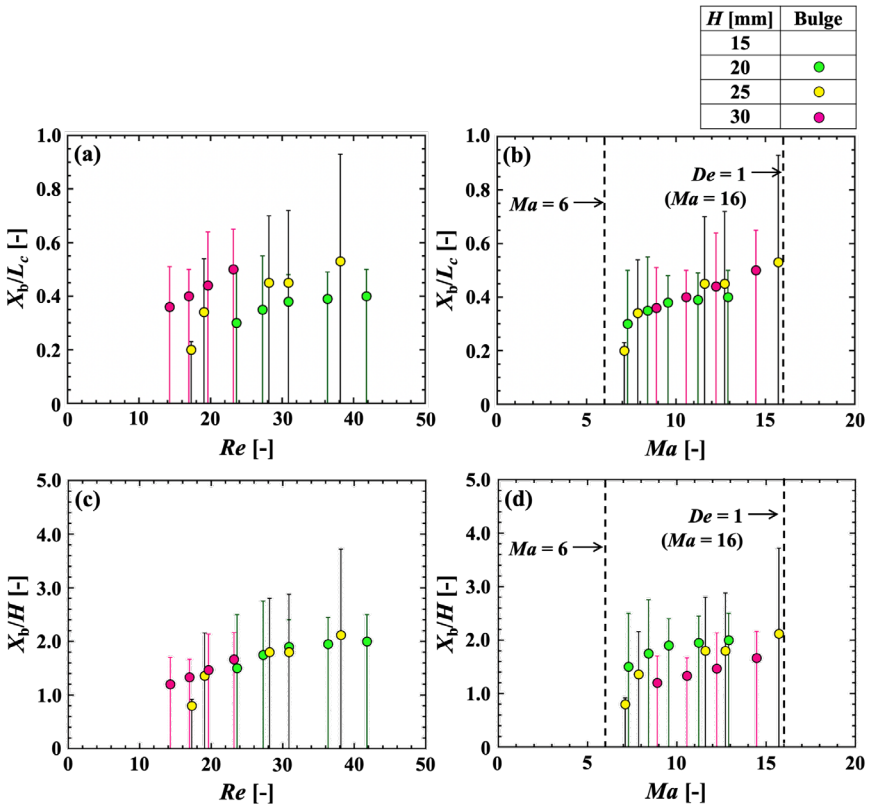

Fig. 17. Length of the bulge structure X_b in Channel C with H = 15 – 30 mm normalized by L_c and H plotted as a function of Re and Ma.

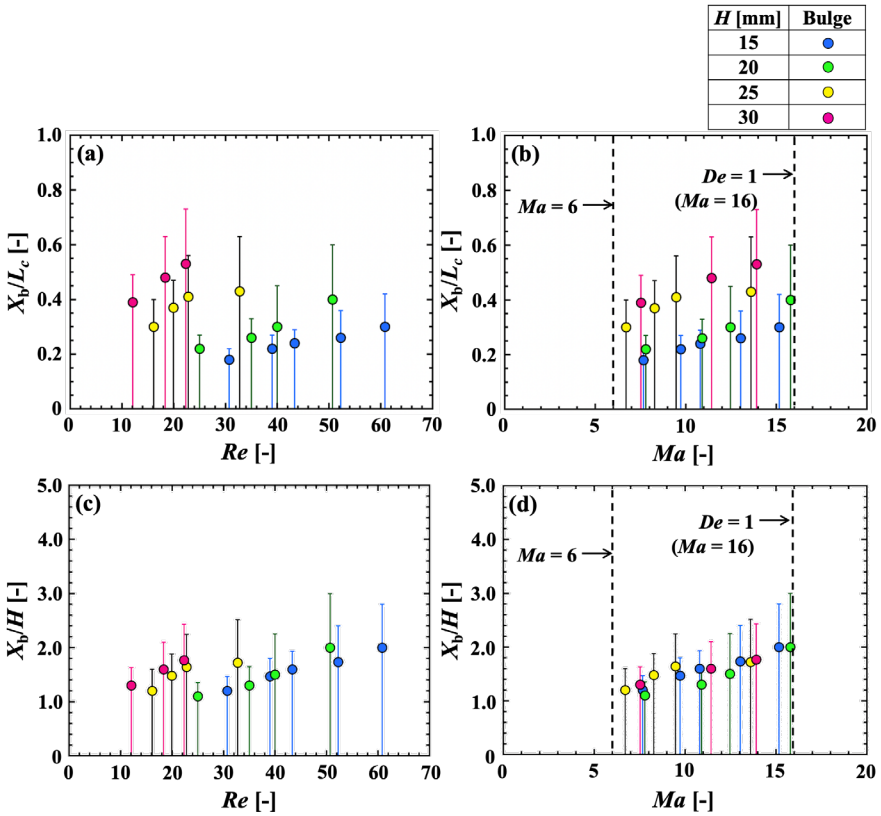

Fig. 18. Length of the bulge structure X_b in Channel D with H = 15 – 30 mm normalized by L_c and H plotted as a function of Re and Ma.

4. Conclusion

This study focused on the effects of the channel geometry on the flow regimes in a cavity. The cavity length, rib length, rib height, and spanwise width of the channel were varied, which influenced the enhancement and relaxation processes of the wormlike micelles and dimensionless numbers of fluids. The flow regimes were categorized as the Barus effect flow, bulge structure, and separation flow. These flows were characterized by a Re–Wi space, and the transitions of these flow regimes were described by Ma and De in almost all channels, except Channel C with H=15, which confirmed that the flow was affected by both inertia and elasticity. Therefore, the characteristic flow structure was well described by Ma instead of Re, particularly for the reattachment length X_r. The development of X_r indicated that the bulge structure quickly shortened the reattachment length. Conversely, the separation length X_s was not significantly affected by Ma. Therefore, in the flow regime affected by the Barus effect, we consider the force balances that may affect X_s based on the pressure gradient and extensional stresses

calculated by assuming an extensional rate. The normalized separation length, X_s/H, is expressed by Eq. (14), which agrees the experimental data for the flow regime of the Barus effect. However, the development of X_s/H expressed by Eq. (14) deviated from the expected value in the flow regime of the bulge structure, which indicates that the bulge structure was a unique phenomenon within the cavity. We also found that X_r and X_s were influenced by the interaction between the flow entering and leaving the cavity, respectively. The length of the bulge structure X_b was well characterized by the rib height, X_b/H, as a function of Ma. In conclusion, this study describes the flow characteristics of cavities in several flow channels. The development of X_r and X_s was characterized by dimensionless numbers in the flow regime of the Barus effect, but the characteristic lengths drastically changed in the bulge structure region. The bulge structure is a unique flow regime that helps to reduce the recirculating regions in the cavity and enhance mixing in the cavity, thereby increasing the heat transfer efficiency in the cavity.

Acknowledgments

This study was supported in part by a Grant-in-Aid for Scientific Research (B) (Project No. 19H02497) from the Japan Society for the Promotion of Science (JSPS KAKENHI) and by the Japan Science and Technology Agency (JST) FOREST Program (Grant Number JPMJFR203O, Japan).

Reference

[1] P.J. Cable, D.V. Boger, A Comprehensive Experimental Investigation of Tubular Entry Flow of Viscoelastic Fluids. Part1. Vortex Characteristics in Stable Flow, AIChE J. 24 (1978) 869-879.

[2] P.J. Cable, D.V. Boger, A Comprehensive Experimental Investigation of Tubular Entry Flow of Viscoelastic Fluids. Part2. The Velocity Field in Stable Flow, AIChE J. 24 (1978) 992-999.

[3] P.J. Cable, D.V. Boger, A Comprehensive Experimental Investigation of Tubular Entry Flow of Viscoelastic Fluids. Part3. Unstable Flow, AIChE J. 25 (1979) 152-159.

[4] S.A. White, A.D. Gotsis, D.G. Baird, Review of The Entry Problem: Experimental and Numerical, J. Non-Newtonian Fluid Mech. 24 (1987) 121-160.

[5] D.V. Boger, D.U. Hur, R.J. Binnington, Futher Observations of Elastic Effects in Tubular Entry Flows, J. Non-Newtonian Fluid Mech. 20 (1986) 31-49.

[6] R.E. Evans, K. Walters, Futher Remarks on The Lip-Vortex Mechanism of Vortex Enhancement in Planar-Contraction Flows, J. Non-Newtonian Fluid Mech. 32 (1989) 95-105.

[7] D.V. Boger, Viscoelastic Flows Through Contractions, Ann.Rev. Fluid Mech. 19 (1987) 157-182.

[8] D.V. Boger, R.J. Binnington, Circular Entry Flows of Fluid M1, J. Non-Newtonian Fluid Mech. 35 (1990) 339-360.

[9] K. Chiba, T. Sakatani, K. Nakamura, Anomalous Flow Patterns in Viscoelastic Entry Flow Through a Planar Contraction, J. Non-Newtonian Fluid Mech. 36 (1990) 193-203.

[10] K. Chiba, S. Tanaka, K. Nakamura, The Structure of Anomalous Entry Flow Patterns Through a Planar Contraction, J. Non-Newtonian Fluid Mech. 42 (1992) 315-322.

[11] J.P. Rothstein, G.H. McKinley, Extensional flow of a polystyrene Boger fluid through a 4:1:4 axisymmetric contraction / expansion, J. Non-Newtonian Fluid Mech. 86 (1999) 61-88.

[12] J.P. Rothstein, G.H. McKinley, The axisymmetric contraction–expansion: the role of extensional rheology on vortex growth dynamics and the enhanced pressure drop, J. Non-Newtonian Fluid Mech. 98 (2001) 33-63.

[13] L.E. Rodd, T.P. Scott, D.V. Boger, J.J.C. White, G.H. McKinley, The inertio-elastic planar entry flow of low-viscosity elastic fluids in micro-fabricated geometries, J. Non-Newtonian Fluid Mech. 129 (2005) 1-22.

[14] L.E. Rodd, J.J.C. White, D.V. Boger, G.H. McKinley, Role of the elasticity number in the entry flow of dilute polymer solutions in micro-fabricated contraction geometries, J. Non-Newtonian Fluid Mech. 143 (2007) 170-191.

[15] E. Miller, J.J.C. White, The effects of chain conformation in the microfluidic entry flow of polymer–surfactant systems, J. Non-Newtonian Fluid Mech. 160 (2009) 22-30.

[16] L.E. Rodd, D. Lee, K.H. Ahn, J.J.C. White, The importance of downstream events in microfluidic viscoelastic entry flows: Consequences of increasing the constriction length, J. Non-Newtonian Fluid Mech. 165 (2010) 1189-1203.

[17] Z. Li, X.F. Yuan, S.J. Haward, J.A. Odell, S. Yeates, Non-linear dynamics of semi-dilute polydisperse polymer solutions in microfluidics: A study of a benchmark flow problem, J. Non-Newtonian Fluid Mech. 166 (2011) 951-963.

[18] A. Lanzaro, X.F. Yuan, Effects of contraction ratio on non-linear dynamics of semi-dilute, highly polydisperse PAAm solutions in microfluidics, J. Non-Newtonian Fluid Mech. 166 (2011) 1064-1075.

[19] A. Lanzaro, X.F. Yuan, A quantitative analysis of spatial extensional rate distribution in nonlinear viscoelastic flows, J. Non-Newtonian Fluid Mech. 207 (2014) 32-41.

[20] R.Hidema, T. Oka, Y. Komoda, H. Suzuki, Effects of flexibility and entanglement of sodium hyaluronate in solutions on the entry flow in micro abrupt contraction-expansion channels, Phys. Fluids 31 (2019) 72005.

[21] H. Nguyen, D.V. Boger, The kinematics and stability of die entry flows, J. Non-Newtonian Fluid Mech. 5 (1979) 353-368.

[22] M.A. Alves, P.J. Oliveira, F.T. Pinho, On the effect of contraction ratio in viscoelastic flow through abrupt contractions, J. Non-Newtonian Fluid Mech. 122 (2004) 117-130.

[23] M.A. Alves, F.T. Pinho, P.J. Oliveira, Visualizations of Boger Fluid Flows in a 4:1 Square–Square Contraction, AIChE J. 51 (2005) 2908-2922.

[24] P.C. Sousa, P.M. Coelho, M.S.N. Oliveira, M.A. Alves, Three-dimensional flow of Newtonian and Boger fluids in square–square contractions, J. Non-Newtonian Fluid Mech. 160 (2009) 122-139.
[25] R.E. Evans, K. Walters, Flow characteristics associated with abrupt changes in geometry in the case of highly elastic liquids, J. Non-Newtonian Fluid Mech. 20 (1986) 11-29.
[26] X. Hu, P.E. Boukany, O.L. Hemminger, L.J. Lee, The Use of Microfluidics in Rheology, Macromol. Mater. Eng. 296 (2011) 308-320.
[27] S.J. Haward, T.J. Ober, M.S.N. Oliveira, M. A. Alves, G.H. McKinley, Extensional rheology and elastic instabilities of a wormlike micellar solution in a microfluidic cross-slot device, Soft Matt. 8 (2012) 536-555.
[28] S.J. Haward, G.H. McKinley, A.Q. Shen, Elastic instabilities in planar elongational flow of monodisperse polymer solutions, Sci. Rep. 6 (2016) 33029.
[29] A. Groisman, S.R. Quake, A Microfluidic Rectifier: Anisotropic Flow Resistance at Low Reynolds Numbers, Phys. Rev. Lett. 92 (2004) 94591.
[30] C.J. Pipe, G.H. McKinley, Microfluidic rheometry, Mech. Res. Commun. 36 (2009) 110-120.
[31] T.J. Ober, S.J. Haward, C.J. Pipe, J. Soulages, G.H. McKinley, Microfluidic extensional rheometry using a hyperbolic contraction geometry, Rheol. Acta. 52 (2013) 529-546.
[32] H.S. Lee, S.J. Muller, A differential pressure extensional rheometer on a chip with fully developed elongational flow, J. Rheol. 61 (2017) 1049.
[33] S.G. Kim, C.M. Ok, H.S. Lee, Steady-state extensional viscosity of a linear polymer solution using a differential pressure extensional rheometer on a chip, J. Rheol. 62 (2018) 1261.
[34] P. Pakdel, G.H. McKinley, Elastic Instability and Curved Streamlines, Phys. Rev. Lett. 77 (1996) 2459-2462.
[35] G.H. McKinley, P. Pakdel, A. Öztekin, Rheological and geometric scaling of purely elastic flow instabilities, J. Non-Newtonian Fluid Mech. 67 (1996) 19-47.
[36] S. Kenney, K. Poper, G. Chapagain, G.F. Christopher, Large Deborah number flows around confined microfluidic cylinders, Rheol. Acta. 52 (2013) 485-497.
[37] X. Shi, S. Kenney, G. Chapagain, G.F. Christopher, Mechanisms of onset for moderate Mach number instabilities of viscoelastic flows around confined cylinders, Rheol. Acta. 54 (2015) 805-815.
[38] S.J. Haward, J. Page, T.A. Zaki, A.Q. Shen, "Phase diagram" for viscoelastic Poiseuille flow over a wavy surface, Phys. Fluids. 30 (2018) 113101.
[39] N. Burshtein, A.Q. Shen, S.J. Haward, Controlled symmetry breaking and vortex dynamics in intersecting flows, Phys. Fluids. 31 (2019) 34104.
[40] M.K. Raihan, S. Wu,Y. Songb, X. Xuan, Constriction length dependent instabilities in the microfluidic entry flow of polymer solutions, Soft Matter 17 (2021) 9198-9209.
[41] H. Suzuki, S. Kida, T. Nakamae, K. Suzuki, Flow and heat transfer over a backward-facing step with a cylinder mounted near its top corner, Int. J. Heat Fluid Flow 12 (1991) 363-359.
[42] J.H. Xu, S. Zou, K. Inaoka, G.N. Xi, Effect of Reynolds number on flow and heat transfer in incompressible forced convection over a 3D backward-facing step, Int. J. Refrig. 79 (2017) 164-175.

[43] Castro, F.T. Pinho, Turbulent expansion flow of low molecular weight shear-thinning solutions, Exp. Fluids 20 (1995) 42-55.
[44] B. Pak, Y.I. Cho, S.U.S. Choi, Separation and reattachment of non-newtonian fluid flows in a sudden expansion pipe, J. Non-Newtonian Fluid Mech. 37 (1990) 175-199.
[45] A.S. Pereira, F.T. Pinho, Turbulent characteristics of shear-thinning fluids in recirculating flows, Exp. Fluids 28 (2000) 266-278.
[46] M.P. Escudier, S. Smith, Turbulent flow of Newtonian and shear-thinning liquids through a sudden axisymmetric expansion, Exp. Fluids 27 (1999) 427-434.
[47] A. Spereira, F.T. Pinho, Recirculating turbulent flows of thixotropic fluids, J. Non-Newtonian Fluid Mech. 99 (2001) 183-201.
[48] R.J. Poole, M.P. Escudier, Turbulent flow of non-Newtonian liquids over a backward-facing step: Part I. A thixotropic and shear-thinning liquid, J. Non-Newtonian Fluid Mech. 109 (2003) 177-191.
[49] R.J. Poole, M.P. Escudier, Turbulent flow of non-Newtonian liquids over a backward-facing step: Part II. Viscoelastic and shear-thinning liquids, J. Non-Newtonian Fluid Mech. 109 (2003) 193-230.
[50] R.J. Poole, M.P. Escudier, Laminar flow of a viscoelastic shear-thinning liquid over a backward-facing step preceded by a gradual contraction, Phys. Fluids. 19 (2007) 93101.
[51] S. Wu, M.K. Raihan, L. Song, X. Shao, J.B. Bostwick, L. Yu, X. Pan, X. Xuan, Polymer effects on viscoelastic fluid flows in a planar constriction microchannel, J. Non-Newtonian Fluid Mech. 290 (2021) 104508.
[52] F.J.G. Rosales, L.C. Deano, F.T. Pinho, E.V. Bokhorst, P.J. Hamersma, M.S.N. Oliveira, M.A. Alves, Microfluidic systems for the analysis of viscoelastic fluid flow phenomena in porous media, Microfluid Nanofluidics 12 (2012) 485-498.
[53] F.J. Galindo-Rosales, L. Campo-Deaño, P.C. Sousa, V.M. Ribeiro, M.S.N. Oliveira, M.A. Alves, F.T. Pinho, Viscoelastic instabilities in micro-scale flows, Exp. Therm. Fluid Sci. 59 (2014) 128-139.
[54] C. Sasmal, Flow of wormlike micellar solutions through a long micropore with step expansion and contraction, Phys. Fluids. 32 (2020) 013103.
[55] H. Suzuki, R. Hidema, K. Tanomura, Y. Komoda, K. Suzuki, Velocity fields around the bulge structure observed in a cavity swept by a visco-elastic fluid, Nihon Reoroji Gakkaishi 46 (2018) 29-36.
[56] H. Suzuki, R. Hidema, Y. Komoda, Flow Characteristics in a Micro-Cavity Swept by a Visco-Elastic Fluid, Exp. Therm. Fluid Sci. 67 (2015) 96-101.
[57] H. Sato, H. Suzuki, R. Hidema, Y. Komoda, Effects of the Molar Ratio of Counter-Ions on Flow Characteristics of Surfactant Solutions Sweeping Cavities, Nihon Reoroji Gakkaishi 44 (2016) 143-151.
[58] H. Suzuki, H. Sato, R. Hidema, Y. Komoda, Bulge Structure in a Cavity Swept by a Viscoelastic Fluid, J. Phys. Conf. Ser. 530 (2014) 12055.
[59] S. Gulati, S.J. Muller, D. Liepmann, Direct measurements of viscoelastic flows of DNA in a 2:1 abrupt planar micro-contraction, J. Non-Newtonian Fluid Mech. 155 (2008) 51-66.

[60] H. Suzuki, Y. Higuchi, H. Watanabe, Y. Komoda, S. Ozawa, T. Nishimura, N. Takenaka, Relaxation Behavior of a Drag-Reducing Cationic Surfactant Solution, Nihon Reoroji Gakkaishi 40 (2012) 85-90.
[61] E. Miller, J.J.C. White, The effects of chain conformation in the microfluidic entry flow of polymer–surfactant systems, J. Non-Newtonian Fluid Mech. 160 (2009) 22-30.
[62] S.C. Omowunmi, X.F. Yuan, Modelling the three-dimensional flow of a semi-dilute polymer solution in microfluidics—on the effect of aspect ratio, Rheol. Acta. 49 (2010) 585-595.
[63] A. Lanzaro, Z. Li, X.F. Yuan, Quantitative characterization of high molecular weight polymer solutions in microfluidic hyperbolic contraction flow, Microfluid Nanofluidics 18 (2015) 819-828.
[64] K. Fukushima, H. Kishi, H. Suzuki, R. Hidema, Modification of turbulence caused by cationic surfactant wormlike micellar structures in two-dimensional turbulent flow, J. Fluid Mech., 933 (2022) A9.
[65] R. J. Poole, The Deborah and Weissenberg numbers. Rheol. Bull., 53, (2012) 32-39.
[66] H. -P. Nguyen, K. Ishihara, H. Suzuki, Y. Kawaguchi, H. Usui, Biaxial extensional characteristics of drag-reducing surfactant solution, Nihon Reoroji Gakkaishi (J. Soci. Rheol. Japan), 33 (2005) 145.